Research Article

Wear and breakage of coated carbide tool in milling of H13 steel and SKD11 hardened steel

Feng Gong[1] · Jun Zhao[2] · Xiuying Ni[1] · Changxia Liu[1] · Junlong Sun[1] · Quanzhong Zhang[1]

Abstract

In the present paper, the wear and breakage mechanisms of coated carbide tools are investigated in milling of H13 steel (HRC 30–35) and SKD11 hardened steel (HRC 58–62). The experiment results indicate that the hardness of workpiece has a dominant effect on tool failure patterns. Due to the low hardness of H13 steel, low-stress-repeated impact load on the tool induces the generation of cracks, but not enough to cause tool fracture. Thus, tool failure pattern is flank wear in milling of H13 steel. In contrast, the high-stress-repeated impact load facilitates the initiation and propagation of cracks and ultimately leads to breakage of rake face when milling SKD11 hardened steel. The geometry model of tool wear and breakage is established to explore the variation of tool angle. It is found that the flank wear reduces the clearance angle, while the breakage of rake face decreases the rake angle. In addition, the effect of tool wear and breakage on the cutting forces and chip formation is studied. The flank wear increases the friction coefficient between tool and H13 steel, and the breakage of rake face increases chip deformation and reduces the sharpness of cutting edge, both of which result in the increase in cutting forces. Furthermore, the wave-shaped chips are formed throughout milling of H13 steel, while the breakage of rake face results in the curling and separation of sawtooth chips when milling SKD11 hardened steel.

Keywords Coated carbide tool · Tool wear and breakage · Cutting forces · Chip formation

1 Introduction

High-speed machining (HSM), which has high efficiency, high quality and low consumption, has been widely applied in the field of manufacturing industry [1]. However, the realization of high-speed machining requires the tools that have excellent cutting performance [2]. The coated carbide tools have broad application in high-speed machining because of their desirable properties such as high hardness, low friction coefficient, outstanding chemical stability and favorable economy [3, 4].

Several researches have been carried out to demonstrate the excellent cutting performance of coated carbide tools. Sharif et al. [5] investigated the cutting performance of coated- and uncoated-carbide tools in drilling titanium alloy-Ti–6Al4V. The results showed that the coated tools significantly outperformed uncoated tools in terms of tool life and surface finish. Song et al. [6] compared the cutting performance of MoS2/Zr-coated carbide tools and uncoated tools in turning 45 hardened steel. It was found that coated carbide tools reduced the shear stress of tool surface, which decreased cutting forces and increased the resistance of wear. Sahoo et al. [7] studied the tool failure mechanisms in turning of 4340 steel using uncoated and multilayer-coated carbide tools. The results revealed that the failure mechanism of the uncoated tools was chipping due to the shortage of mechanical strength, while the multilayer-coated carbide tools had a steady wear growth. Ginting et al. [8] verified that the coated carbide tools reduced the machined surface roughness because of its high hardness and low friction coefficient.

To further improve the cutting performance of coated carbide tools, the failure patterns and mechanisms of coated carbide tools were studied by scholars. Jawaid et al. [9] proved that the chipping and flaking on the rake face were the failure patterns of coated carbide tools when milling titanium alloy. Ezugwu et al. [10] analyzed the failure mechanisms of TiN-coated tools in intermittent turning EN 19T steel. The results indicated that abrasive wear and plastic deformation of cutting edge were the tool failure mechanisms at high cutting conditions. Suresh et al. [11] found that the abrasive wear was the principle failure mechanism of coated carbide tools in turning hardened steel 4340 (HRC 48). Hao et al. [12] presented that the failure mechanism of coated carbide tools was adhesive wear at low cutting speeds in turning Inconel 718, while oxidative wear dominated the tool failure mechanisms at high cutting speeds. Li et al. [13] studied the coated carbide tool failure propagation in end milling of Inconel 718 and found that the predominant tool failure pattern was flank wear. Çalışkan et al. [14, 15] reported that dominant failures mechanisms of coated carbide tools were abrasive and adhesive wear in milling of Ti6Al4V and found that abrasive and oxidative wear were dominant tool failure patterns in milling of hardened AISI O2 steel. Corrêa [16] confirmed that abrasion and diffusion wear were the tool failure patterns in machining of martensitic stainless steels, while attrition and abrasion wear were dominant tool failure patterns for the supermartensitic stainless steel. It can be concluded that the wear is the dominant failure pattern of coated carbide tool.

However, the breakage occurs when the coated carbide tools are subject to strong impact load. Li et al. [17] presented the failure mechanisms of coated carbide tool for milling Ti–6Al–4V alloy. The results showed that the breakage caused by deformation of cutting edge was tool main failure mechanism at high speeds. Ghani et al. [18] found that the crack initiated and propagated at the cutting edge due to the effect of cyclic loading in intermittent milling titanium alloy. Wang et al. [19] investigated the failure mechanisms of coated carbide tool in milling Ti–6Al–4V based on the finite element method and found that the tool failure mechanism was brittle fracture.

It is well known that tool basis failure patterns are wear and breakage. However, few studies focus on the condition in which tool wear and breakage occur. In our previous research, the effect of cutting speeds on the failure patterns of coated carbide tools was investigated in milling SKD11 hardened steel [20]. It was found that tool failure pattern was fatigue fracture. However, the cracks propagation paths were concerned and the reasons why the cracks propagate steadily and result in tool fracture were ignored before. In the present paper, the milling experiments of H13 steel and SKD11 hardened steel were conducted to investigate the mechanisms of tool wear and breakage. The geometry model of tool wear and breakage was established to explore the variation of tool angle. In addition, the effect of tool wear and breakage on cutting forces and chip formation is explored.

2 Experimental procedures

### 2.1 Workpiece materials and cutting tools

To explore the effect of workpiece materials on tool failure patterns, the milling experiments were performed on H13 steel (HRC 30–35) and SKD11 hardened steel (HRC 58–62), respectively. The hardness of workpieces was tested by the portable hardness tester (HM-6580). The workpiece materials were processed into rectangular blocks with the length and width of 100 mm and 75 mm. The chemical compositions of the H13 steel and SKD11 hardened steel are shown in Table 1. The cemented carbide tools with CVD-coated double-layer Al_2O_3/Ti(C,N) (Seco MP1500) were adopted throughout the milling experiments. The structure of the coated carbide tool is seen from Fig. 1, including the shape of tool and the order and thickness of the coating layer. The R220.53-0125-09-8C tool holder manufactured by Seco Tools with a diameter of 125 mm was employed with tool geometry as follows: axial rake angle of 20°, radial rake angle of −5° and major cutting edge angle of 45°.

2.2 Cutting tests

The CNC milling machine of DAEWOO ACE-V500 with the range of spindle speed from 80 to 10,000 rpm was used in the present experiment. The previous researches showed

Table 1 Chemical composition of workpieces (wt %) [21, 22]

Workpieces	Element wt%								
	C	Si	Mn	Cr	Mo	V	P	S	Fe
H13 steel	0.32–0.45	0.80–1.20	0.20–0.50	4.75–5.50	1.10–1.75	0.80–1.20	≤0.03	≤0.03	Balance
SKD11 hardened steel	1.4–1.6	≤0.6	≤0.6	11.0–13.0	0.7–1.2	0.15–0.3	–	–	

Fig. 1 The structure of coated carbide tool
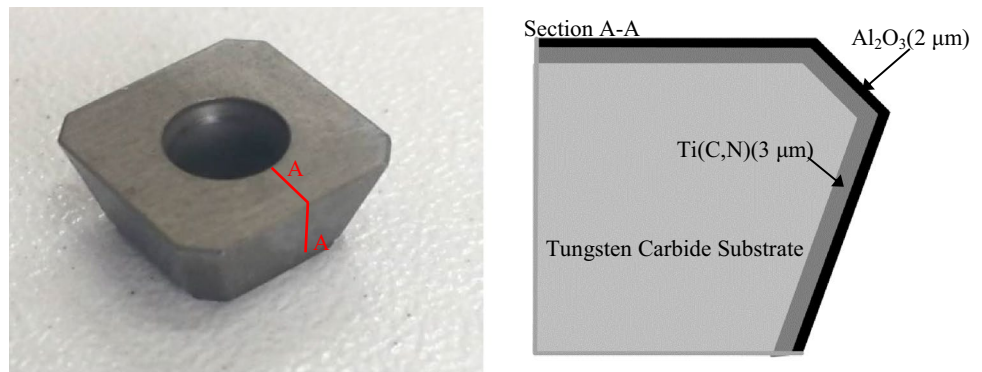
Table 2 Cutting parameters of milling experiments

Workpiece	fixed parameter	variable parameter	variable value
H13 steel	$v_c = 900$ m/min, $f = 0.15$ mm/z, $a_e = 75$ mm	a_p (mm)	0.30, 0.50, 0.70, 0.90, 1.10
SKD11 hardened steel	$v_c = 120$ m/min, $f = 0.05$ mm/z, $a_e = 75$ mm	a_p (mm)	0.07, 0.10, 0.13, 0.16

that the cutting depths had a great effect on tool cutting performance when cutting hardened steel [23, 24]. Therefore, the single-factor experiments with cutting depths variables were conducted to explore the mechanisms of tool wear and breakage. Due to the different hardness of two workpieces materials, the cutting depths ranging from 0.3 to 1.1 mm in steps of 0.2 mm were adopted in milling H13 steel, while it increased from 0.07 to 0.16 mm in steps of 0.03 mm when milling SKD11 hardened steel as shown in Table 2. For each cutting parameter, only one fresh insert was used, and each condition was repeated twice to avoid the error induced by the differences in cutting performance of the inserts. The symmetric milling was adopted in the experiment.

In order to analyze tool failure process, the condition of tool damage was measured and recorded periodically by tool microscope (AM413ZT) connected to the computer. When the width of flank wear exceeded 0.3 mm or catastrophic breakage occurred at the rake face, the tool was considered as failure. The tool failure surface morphology was examined by scanning electronic microscope (JSM-6510 LV) equipped with an energy-dispersive spectroscopy. For each cutting parameter, the cutting forces were measured by Kistler 9257A three-component piezoelectric dynamometer and the chips were collected, which were used to investigate the effect of tool wear and breakage on cutting forces and chip formation.

3 Results and discussion

3.1 Tool failure patterns and mechanisms

3.1.1 Tool wear in milling of H13 steel

Figure 2 shows the failure surface morphology of coated carbide tool under the cutting depth of 0.3 mm in milling of H13 steel. Due to the low hardness of H13 steel, low-stress-repeated impact load on the tool induces that the tool failure pattern is flank wear and the tool disabled part is located mainly in the tool nose as shown in Fig. 2a. The parallel friction marks scratched by hard particles in workpiece are found on the tool chamfering as shown in Fig. 2b, indicating that the abrasive wear occurs at the tool chamfering. The EDS analysis of point A and B shows that a large amount of Fe, Cr and Si elements, which are the compositions of H13 steel, are detected on the surface of coated carbide tool as shown in Fig. 2d, f, proving the existence of adhesive wear. Besides, the Al and O elements detected on the tool chamfering (point A in Fig. 2b) confirm the presence of Al_2O_3 coating. In addition, the thermal cracks perpendicular to the cutting edge in Fig. 2b and c reveal that the coated carbide tools withstand high thermal stresses at low cutting depth.

Figure 3 exhibits the failure surface morphology of coated carbide tool at $a_p = 0.7$ mm in milling of H13 steel. It is found that the tool failure pattern is also flank wear. Figure 3a shows that the chamfering of the tool is worn out in milling process, which results in the slight wear
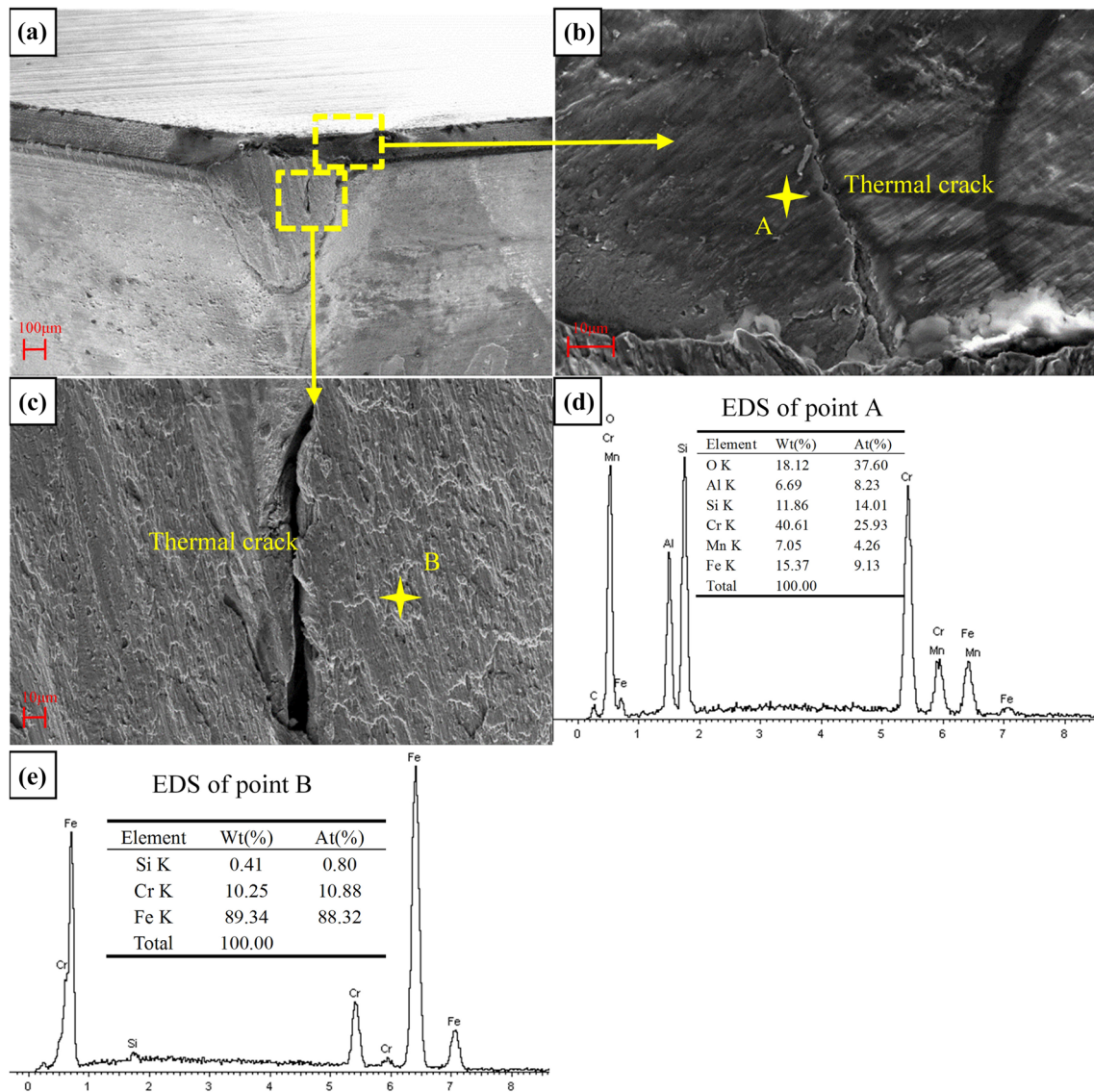
Fig. 2 SEM micrographs and EDS analysis of worn tool in milling H13 steel ($a_p = 0.30$ mm, $v_c = 900$ m/min, $f = 0.15$ mm/z)

of rake face as shown in Fig. 3b. Due to the increase in cutting depth, the coated carbide tools are subjected to larger alternating mechanical impact and the flank wear reduces the performance of coated carbide tool, both of which cause that the mechanical cracks parallel to the cutting edge generate at the exposed substrate of flank face as shown in Fig. 3c. The workpiece materials accumulate on the mechanical cracks, resulting in an increase in the temperature of bonding zone and the generation of thermal cracks. The EDS analysis of point A in Fig. 3c indicates that there is no oxidative wear as shown in Fig. 3d.

The SEM micrographs of worn-coated carbide tool at $a_p = 1.1$ mm are shown in Fig. 4. At higher cutting depth, the severe wear occurs at the flank face as shown in Fig. 4a,

and the area of flank wear is apparently larger compared with that of other cutting depths. The high cutting temperature causes that thermal cracks generate and run through the rake and flank face as shown in Fig. 4b and d. In addition, the severe adhesive wear occurs at the exposed substrate of flank face (Fig. 4c), which increases the roughness of the flank face and worsens cutting conditions. The EDS analysis of point A shows that only O element but no Al element is detected in the adhesion zone, indicating that Al_2O_3 coating is worn and the oxidative wear occurs in virtue of high temperature.
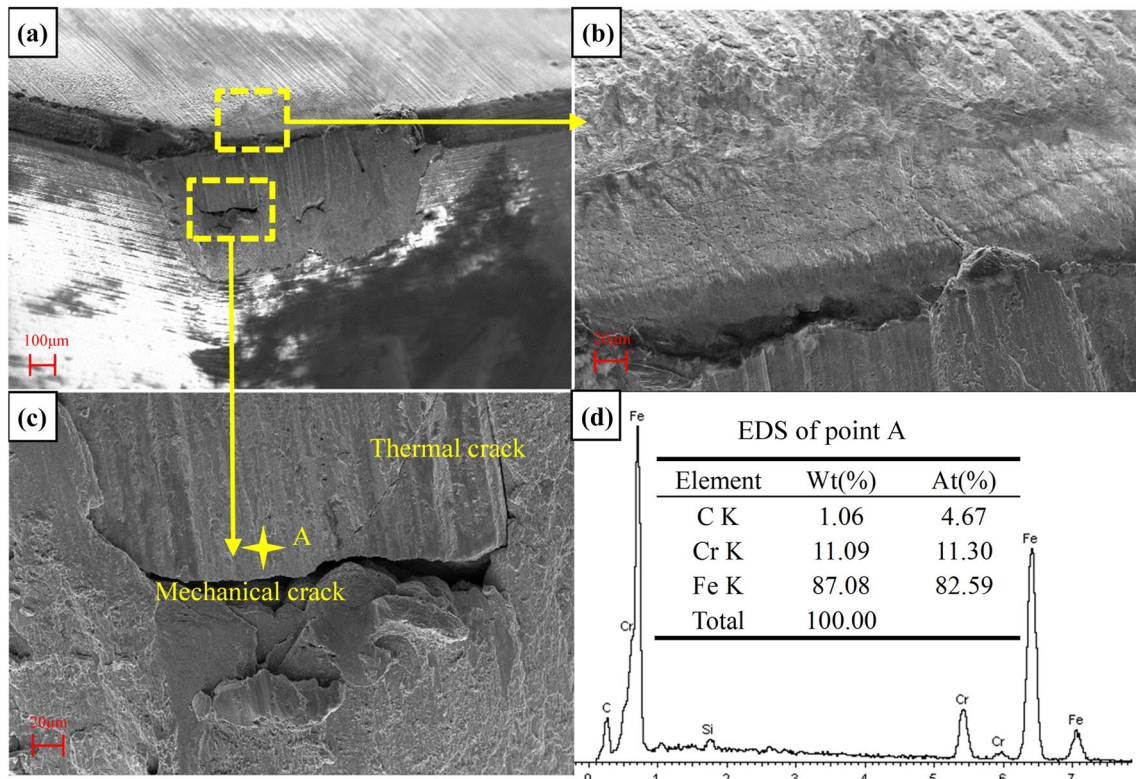
Fig. 3 SEM micrographs and EDS analysis of worn tool in milling H13 steel ($a_p = 0.70$ mm, $v_c = 900$ m/min, $f = 0.15$ mm/z)
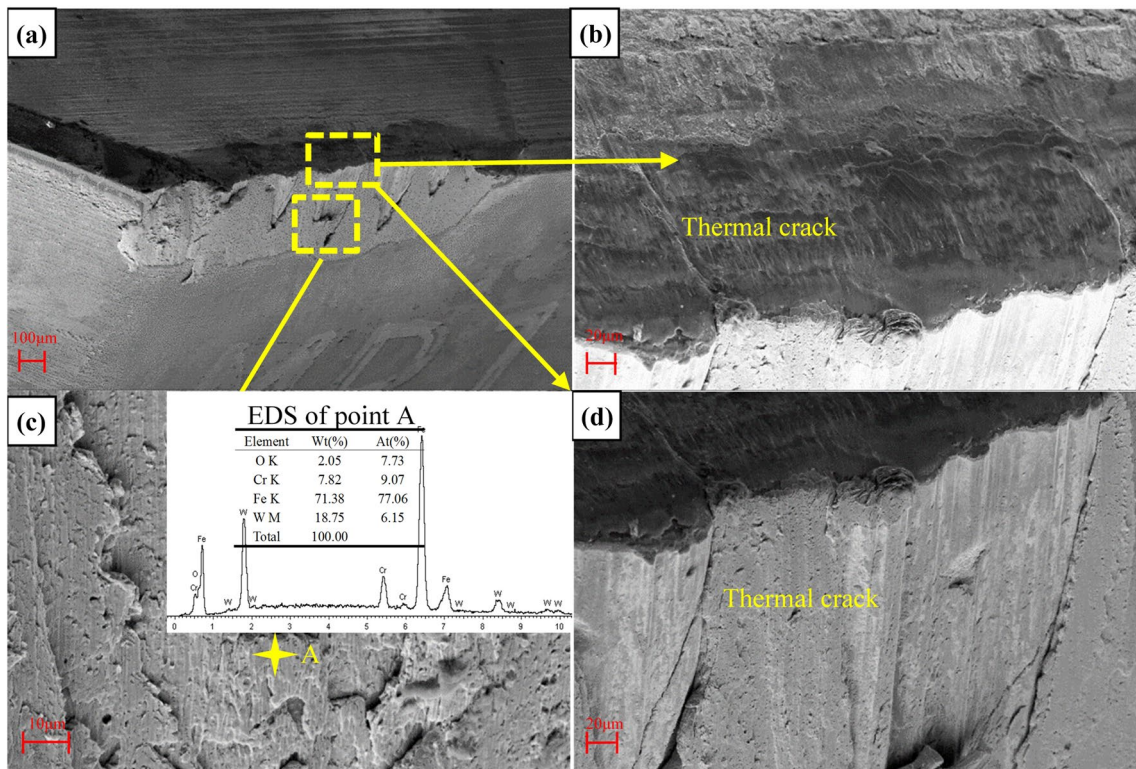
EDS of point A

Element	Wt(%)	At(%)
C K	1.06	4.67
Cr K	11.09	11.30
Fe K	87.08	82.59
Total	100.00	

Fig. 4 SEM micrographs and EDS analysis of worn tool in milling H13 steel ($a_p = 1.1$ mm, $v_c = 900$ m/min, $f = 0.15$ mm/z)

EDS of point A

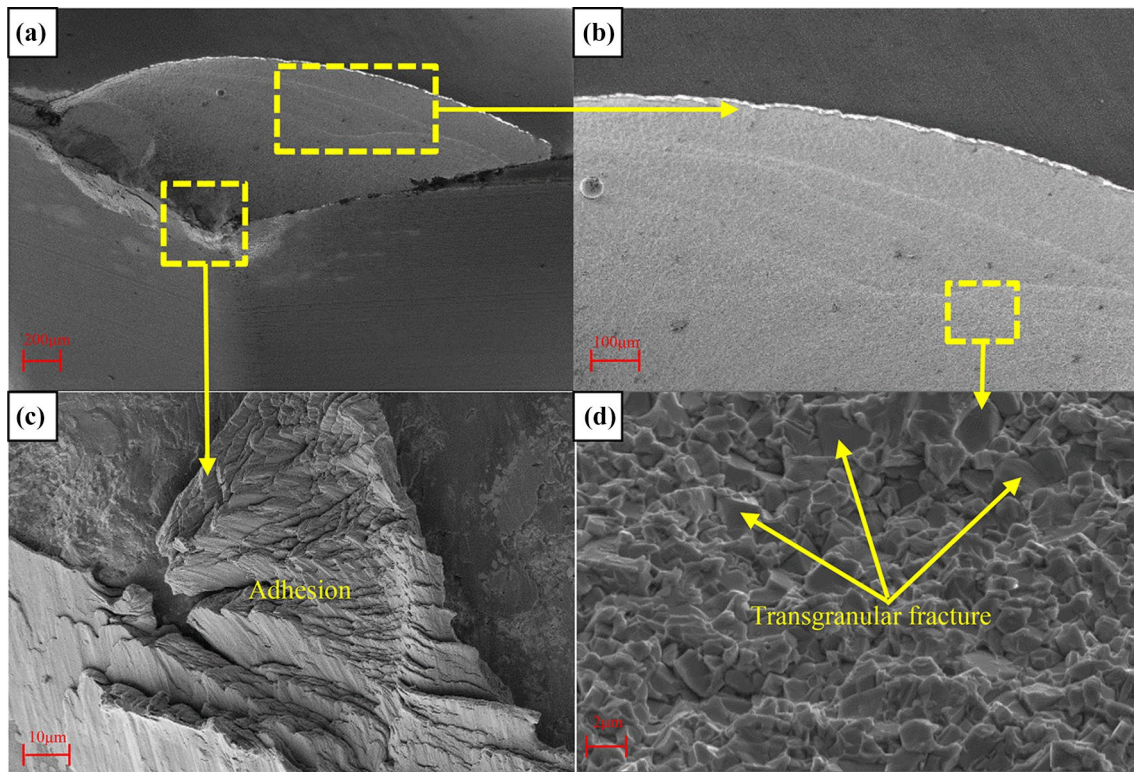| Element	Wt(%)	At(%)
O K	2.05	7.73
Cr K	7.82	9.07
Fe K	71.38	77.06
W M	18.75	6.15
Total	100.00	

Fig. 5 SEM micrographs and EDS analysis of worn tool in milling SKD11 hardened steel ($a_p = 0.07$ mm, $v_c = 120$ m/min, $f = 0.05$ mm/z)

3.1.2 Tool breakage in milling of SKD11 hardened steel

The SEM micrographs of tool failure surface after milling SKD11 hardened steel at $a_p = 0.07$ mm are shown in Fig. 5. On account of the high hardness of SKD11 hardened steel, the coated carbide tools are subjected to strong mechanical impact. The high-stress-repeated impact load on the tool facilitates the initiation and propagation of cracks and ultimately leads to breakage of rake face as shown in Fig. 5a. Because of low cutting depth, the crack propagation region is relatively smooth and the step-shaped fast crack extension region is formed as shown in Fig. 5b. In addition, it can be seen from Fig. 5c that the chips adhere to the minor flank of coated carbide tool as a result of the high hardness of workpiece. The magnified fracture surface of coated carbide tool in Fig. 5d indicates that the fracture mode of coated carbide tool is transgranular fracture at low cutting depth.

Figure 6 exhibits the failure surface of coated carbide tool in milling SKD11 hardened steel at $a_p = 0.10$ mm, from which it can be seen that the tool failure pattern is breakage of rake face. However, the area of the tool fracture surface is smaller than that of $a_p = 0.07$ mm (Fig. 6a). It is attributed to that the higher mechanical impact at $a_p = 0.10$ mm accelerates crack propagation rate and tool failure progress. Because the breakage of rake face exposes

the tool substrate, the wear resistance of coated carbide tools decreases and the friction coefficient between the rake face and chips increases, resulting in the severe abrasion (Fig. 6c) and adhesion (Fig. 6d). The tool fracture mode is also characterized by transgranular fracture as shown in Fig. 6b.

At high cutting depth ($a_p = 0.16$ mm), the appearance of tool failure surface after milling SKD11 hardened steel is shown in Fig. 7. The fatigue steps are observed at the fracture surface (Fig. 7a), indicating that the tool failure mechanisms are fracture caused by the propagation of multiple cracks. Because of the increase in cutting depths, the cutting forces grow large enough to induce the crack initiation at different positions and propagation in fan-wise at different planes (red arrows in Fig. 7a). The height difference between non-coplanar cracks gradually increases in the process of propagation, and the fatigue steps are formed when multiple cracks intersect as shown in Fig. 7b. The cracks adjacent to the fatigue steps in Fig. 7d prove the above analysis. The tool main fracture mode is transgranular fracture as shown in Fig. 7c. In addition, the voids left by grain pull-out indicate that the intergranular fracture also occurs at high cutting depth.

In order to further analyze the effect of tool wear and breakage on variation of tool angle, the two-dimensional geometry model of tool wear and breakage is established
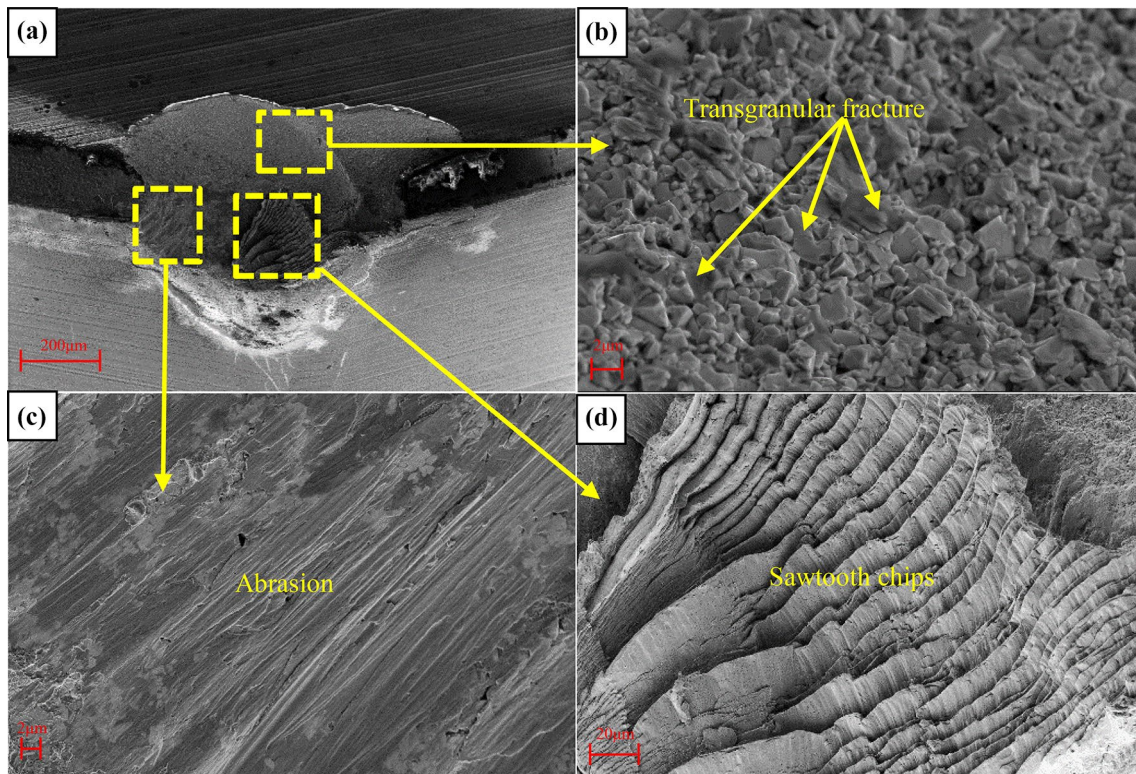
Fig. 6 SEM micrographs and EDS analysis of worn tool in milling SKD11 hardened steel ($a_p = 0.10$ mm, $v_c = 120$ m/min, $f = 0.05$ mm/z)
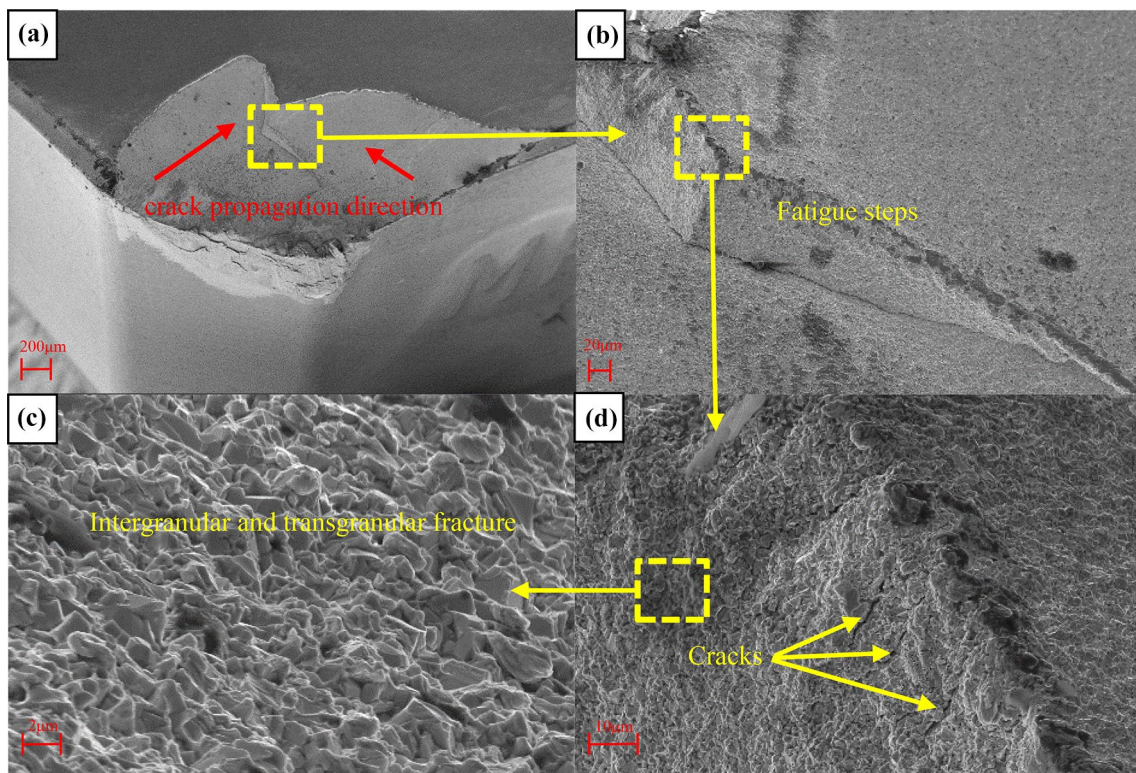

Fig. 7 SEM micrographs and EDS analysis of worn tool in milling SKD11 hardened steel ($a_p = 0.16$ mm, $v_c = 120$ m/min, $f = 0.05$ mm/z)
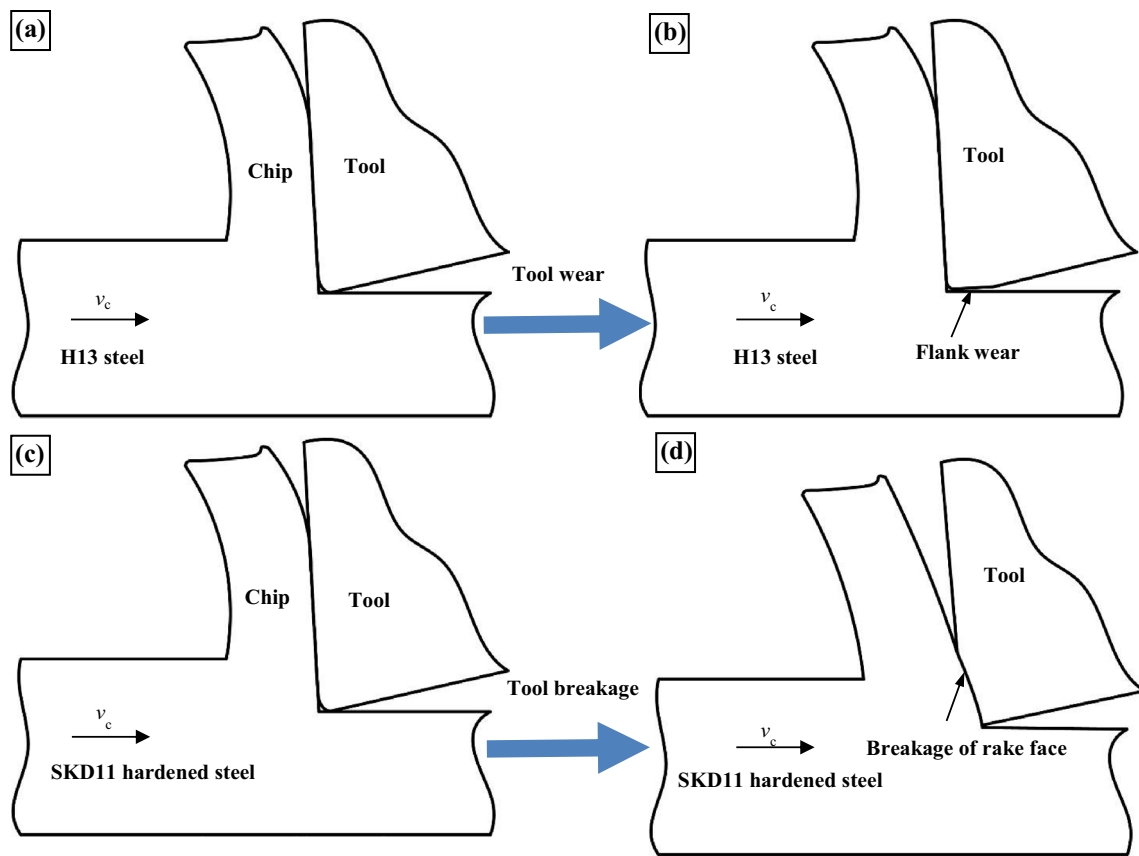
Fig. 8 The two-dimensional geometry model of tool wear and breakage in milling experiments

as shown in Fig. 8. When the tools remain intact, there are same negative rake angle and positive clearance angle in milling of H13 steel and SKD11 hardened steel as shown in Fig. 8a, c. It can be seen from Fig. 8b that the flank wear decreases the clearance angle and increases contact area of the tool-workpiece, which results in that plowing instead of cutting occurs. In addition, the friction coefficient between the tool and workpiece increases due to the damage of coating. However, the breakage of rake face results in severe damage to cutting edge and decreases the rake angle as shown in Fig. 8d. Thus, the tool wear and breakage causes the deterioration of the cutting conditions and has an enormous effect on the cutting forces and chip formation, which will be discussed in the next section.

3.2 Cutting forces

To investigate the effect of tool wear and breakage on the variation of cutting forces, the cutting forces are measured at each pass in milling of H13 steel and SKD11 hardened steel. The steady state cutting forces components in milling H13 steel at $a_p = 0.7$ mm are maintained as shown in Fig. 9. It can be seen that the cutting forces are dynamic and negative cutting forces generate when the tools cut off the workpiece.

The negative shearing leads to the deterioration of stress on the tool and accelerates tool failure. The mean cutting force components F_x, F_y, F_z and resultant cutting force F_r are calculated by using equation shown in Eq. (1) and (2):

$$F_x = \frac{1}{N}\left(\sum_{i=1}^{N} F_{xi}\right), \; F_y = \frac{1}{N}\left(\sum_{i=1}^{N} F_{yi}\right), \; F_z = \frac{1}{N}\left(\sum_{i=1}^{N} F_{zi}\right)$$

(1)

$$F_r = \sqrt{F_x^2 + F_y^2 + F_z^2}$$

(2)

where F_{xi}, F_{yi} and F_{zi} are data sampling value of cutting force in x, y and z directions, respectively.

The cutting force components and resultant cutting forces when milling H13 steel and SKD11 hardened steel at the first pass are shown in Fig. 10. It is found that the cutting force components and resultant cutting forces both increase with the increase in cutting depths. When milling H13 steel, it can be seen in Fig. 10a that the tangential force F_y is the highest, followed by the radial force F_x and axial force F_z. However, the highest cutting force component is axial force F_z and the tangential force F_y is the lowest cutting force component (Fig. 10b) in milling
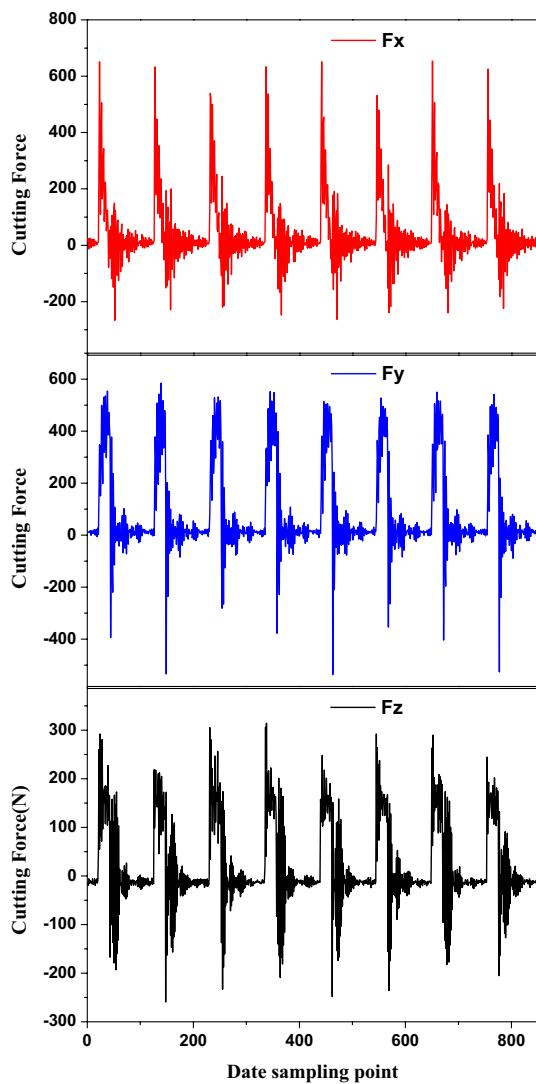
Fig. 9 Cutting forces in milling H13 steel with coated carbide tool at $a_p = 0.7$ mm, $v_c = 900$ m/min, $f = 0.15$ mm/z, $a_e = 75$ mm

SKD11 hardened steel, which is opposite with that of milling H13 steel. It can be concluded that the hardness of workpiece has a dominating effect on the proportion of cutting force components.

Because of the difference of the workpiece and cutting parameters, it is not proper to directly compare the magnitude of cutting forces when milling H13 steel and SKD11 hardened steel. Thus, the growth rate of cutting forces λ is calculated by using equation shown in Eq. (3):

$$\lambda = \frac{(F_l - F_f)}{F_f} \times 100\% \tag{3}$$

where F_f and F_l are the cutting forces obtained at the first and last pass of the workpiece in milling tests, respectively.

The growth rate of cutting forces in milling H13 steel and SKD11 hardened steel is depicted in Fig. 11. As shown in Fig. 11a, the tool wear contributes to that the axial force F_z has the biggest growth in milling H13 steel. It is attribute to that the flank wear reduces the clearance angle and increases the contact area of the tool-workpiece, resulting in that the plowing occurs between the workpiece and tool and axial force F_z grows rapidly. However, the flank wear has no damage to the rake face and cutting edge and cutting performance of coated carbide tool can be maintained. Thus, the tangential cutting force F_y, which is the highest cutting force component at the first pass, has the least growth and becomes the lowest cutting force component.

When milling SKD11 hardened steel, the growth rate of cutting forces caused by breakage of rake face is significantly higher than that induced by tool wear as shown in Fig. 11b. The breakage of rake face decreases the rake face and reduces the sharpness of cutting edge, causing that the growth rate of axial force F_z is larger than that of other cutting forces. In addition, the coating on the tool surface for lubrication and attrition reduction damages and the
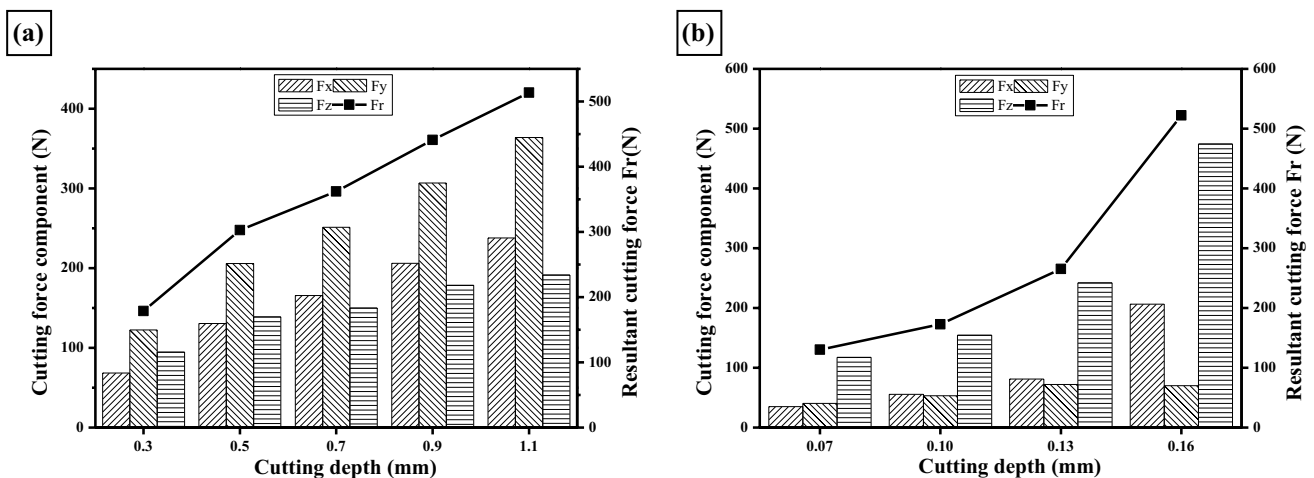

Fig. 10 Cutting force components and resultant cutting forces at first pass **a** milling H13 steel **b** milling SKD11 hardened steel
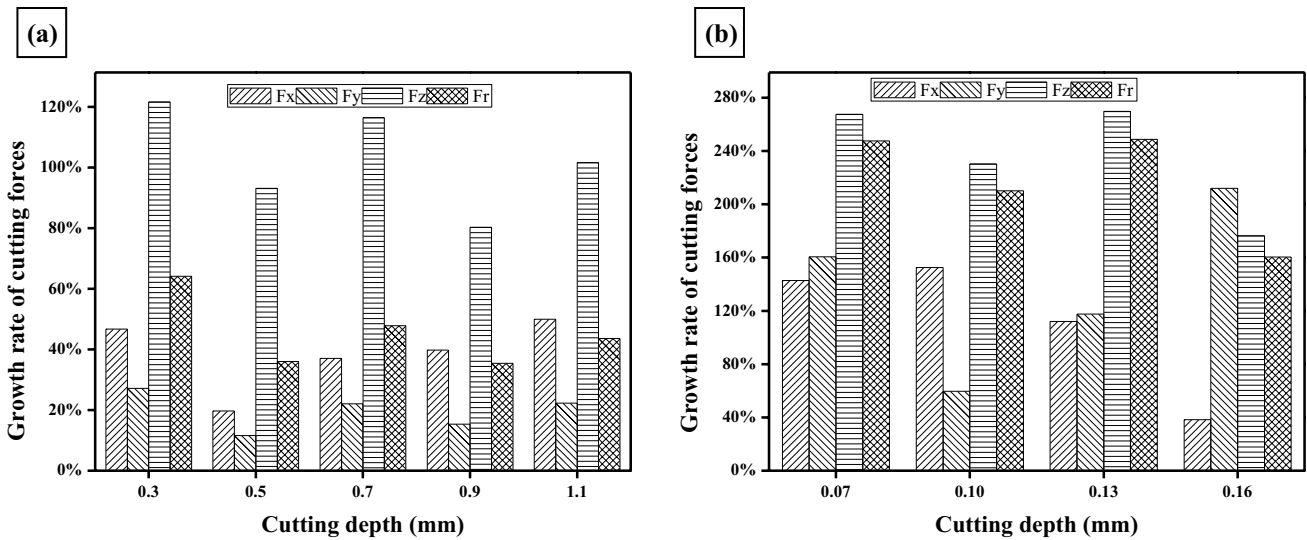
Fig. 11 Growth rate of cutting forces **a** milling H13 steel **b** milling SKD11 hardened steel
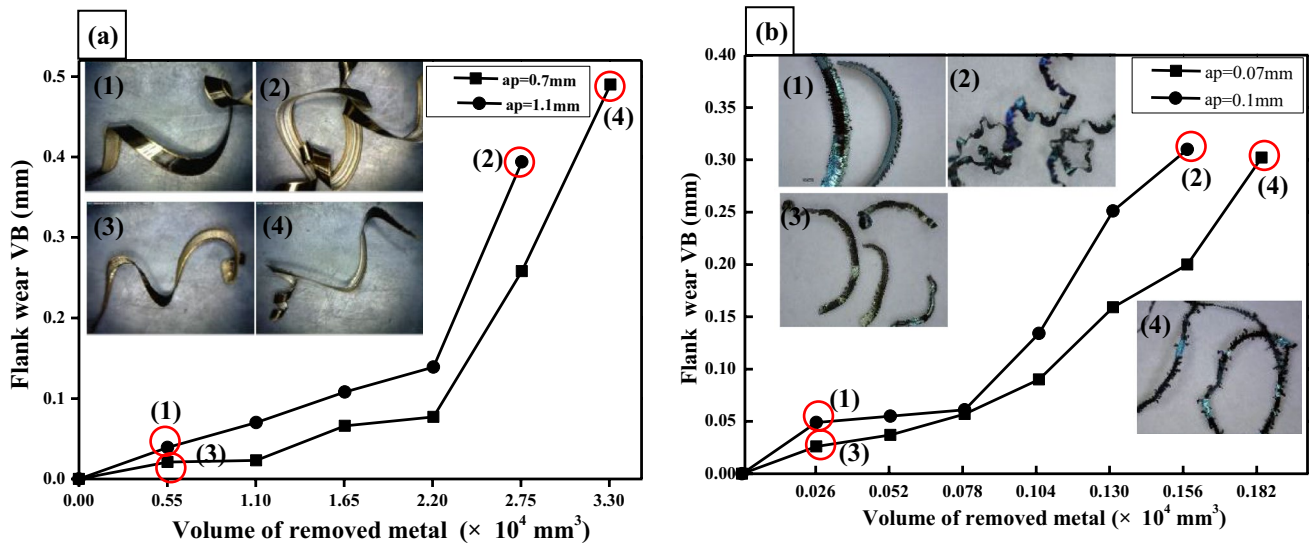

Fig. 12 Evolution of chip formation in milling experiment **a** H13 steel **b** SKD11 hardened steel

substrate is exposed because of the breakage of rake face, increasing the friction coefficient between the exposed substrate and workpiece. Thus, the tangential force F_y has a high growth in milling SKD11 hardened steel.

3.3 Chip formation

The chip formation can reveal important information on the metal cutting process [25]. Thus, to explore the effect of tool wear and breakage on the chip formation, the chips obtained at the first pass and last pass in milling of H13 steel and SKD11 hardened steel under different cutting depths are shown in Fig. 12. It can be seen that

the wave-shaped chips are generated at $a_p = 0.7$ mm and 1.1 mm in milling of H13 steel at the first pass (point 1 and 3 in Fig. 12a). Although the flank wear reduces the clearance angle, the tools have good cutting performance and the contact zone of tool-chip has no change (Fig. 8a). Thus, the chips are still wave-shaped at the last pass of H13 steel (point 2 and 4 in Fig. 12a).

However, when milling SKD11 hardened steel, as a result of the high hardness of workpiece, the sawtooth chips are generated at the first pass of the workpiece (point 1 and 3 in Fig. 12b). However, the breakage of rake face decreases rake angle and tool cutting performance. When the chips slide over the tool rake face, the

deformation of chips increases and vibration of machine tool intensifies, resulting in chip curling and sawtooth separation (point 2 and 4 in Fig. 12b).

4 Conclusion

The milling experiments of H13 steel (HRC 30–35) and SKD11 hardened steel (HRC 58–62) were conducted to investigate the wear and breakage mechanisms of coated carbide tools considering effect of workpiece materials. Besides, the effect of tool wear and breakage on cutting forces and chip formation was also studied. The following conclusions can be drawn:

1. The hardness of workpiece has a dominant effect on tool failure patterns. Due to the low hardness of H13 steel, low-stress-repeated impact load on the tool results in the generation of cracks, but not enough to result in tool fracture. The failure pattern of coated carbide tool is flank wear in milling of H13 steel. However, the high hardness of SKD11 hardened steel results in high-stress-repeated impact load on the tool, which facilitates the initiation and propagation of cracks and ultimately leads to breakage of rake face. The geometry model of tool wear and breakage is established, and the results show that the flank wear reduces the working clearance angle, while the breakage of rake face decreases the working rake angle.

2. The largest cutting force component is tangential force F_y, while axial force F_z ranks last when milling H13 steel with fresh tool. During the milling process, the flank wear reduces the clearance angle and increases the contact area of the tool-workpiece, resulting in that the axial force F_z becomes the largest cutting force component. However, the axial force F_z is the maximum cutting force component in milling SKD11 hardened steel due to its high hardness. The breakage of rake face decreases the rake face and reduces the sharpness of cutting edge. Therefore, the axial force F_z is the maximum cutting force component from beginning to end.

3. During milling H13 steel, the flank wear has no damage to the rake face and the contact zone of tool-chip has no change, which causes that the wave-shaped chip is formed throughout milling process. When milling SKD11 hardened steel with fresh tool, the sawtooth chips are formed. However, the breakage of rake face increases the deformation of chip and intensifies machine tool vibration, resulting in the curling and separation of sawtooth chips.

Compliance with ethical standards

Conflict of interest The authors declare that they have no conflict of interest.

References

1. Cui XB, Zhao J (2014) Cutting performance of coated carbide tools in high-speed face milling of AISI H13 hardened steel. Int J Adv Manuf Technol 71(9–12):1811–1824
2. Tu GZ, Wu SH, Liu J, Long Y, Wang B (2016) Cutting performance and wear mechanisms of Sialon ceramic cutting tools at high speed dry turning of gray cast iron. Int J Refract Met Hard Mater 54:330–334
3. Ciftci I (2006) Machining of austenitic stainless steels using CVD multi-layer coated cemented carbide tools. Tribol Int 39(6):565–569
4. Bobzin K (2017) High-performance coatings for cutting tools. CIRP J Manuf Sci Technol 18:1–9
5. Sharif S, Rahim EA (2007) Performance of coated- and uncoated-carbide tools when drilling titanium alloy—Ti-6Al4V. J Mater Process Technol 185(1–3):72–76
6. Song WL, Deng JX, Zhang H, Yan P (2010) Study on cutting forces and experiment of MoS_2/Zr-coated cemented carbide tool. Int J Adv Manuf Technol 49(9–12):903–909
7. Sahoo AK, Sahoo B (2012) Experimental investigations on machinability aspects in finish hard turning of AISI 4340 steel using uncoated and multilayer coated carbide inserts. Measurement 45(8):2153–2165
8. Ginting A, Skein R, Cuaca D (2018) The characteristics of CVD- and PVD-coated carbide tools in hard turning of AISI 4340. Measurement 129:548–557
9. Jawaid A, Sharif S, Koksal S (2000) Evaluation of wear mechanisms of coated carbide tools when face milling titanium alloy. J Mater Process Technol 99(1):266–274
10. Ezugwu EO, Okeke CI (2001) Tool life and wear mechanisms of TiN coated tools in an intermittent cutting operation. J Mater Process Technol 116(1):10–15
11. Suresh R, Basavarajappa S, Samuel GL (2012) Some studies on hard turning of AISI 4340 steel using multilayer coated carbide tool. Measurement 45(7):1872–1884
12. Hao ZP, Fan YH, Lin JQ, Yu ZX (2015) Wear characteristics and wear control method of PVD-coated carbide tool in turning Inconel 718. Int J Adv Manuf Technol 78(5–8):1329–1336
13. Li HZ, Zeng H, Chen XQ (2006) An experimental study of tool wear and cutting force variation in the end milling of Inconel 718 with coated carbide inserts. J Mater Process Technol 180(1):296–304
14. Çalışkan H, Küçükköse M (2015) The effect of aCN/TiAlN coating on tool wear, cutting force, surface finish and chip morphology in face milling of Ti6Al4V superalloy. Int J Refract Met Hard Mater 50:304–312
15. Çalışkan H, Kurbanoğlu C, Panjan P, Čekada M, Kramar D (2013) Wear behavior and cutting performance of nanostructured hard coatings on cemented carbide cutting tools in hard milling. Tribol Int 62:215–222

16. Corrêa JG, Schroeter RB, Machado ÁR (2017) Tool life and wear mechanism analysis of carbide tools used in the machining of martensitic and supermartensitic stainless steels. Tribol Int 105:102–117

17. Li AH, Zhao J, Luo HB, Pei ZQ, Wang ZM (2012) Progressive tool failure in high-speed dry milling of Ti–6Al–4V alloy with coated carbide tools. Int J Adv Manuf Technol 58(5–8):465–478

18. Ghani JA, Haron CHC, Hamdan SH, Said AYM, Tomadi SH (2013) Failure mode analysis of carbide cutting tools used for machining titanium alloy. Ceram Int 39(4):4449–4456

19. Wang FZ, Zhao J, Li ZL, Li AH (2016) Coated carbide tool failure analysis in high-speed intermittent cutting process based on finite element method. Int J Adv Manuf Technol 83(5–8):805–813

20. Gong F, Zhao J, Jiang YW, Tao HW, Li ZL, Zang J (2017) Fatigue failure of coated carbide tool and its influence on cutting performance in face milling SKD11 hardened steel. Int J Refract Met Hard Mater 64:27–34

21. Wang B, Liu ZQ (2016) Cutting performance of solid ceramic end milling tools in machining hardened AISI H13 steel. Int J Refract Met Hard Mater 55:24–32

22. Wang CY, Ding F, Tang DW (2016) Modeling and simulation of the high-speed milling of SKD11 hardened steel (62 HRC) based on SHPB technology. Int J Mach Tool Manuf 108:13–26

23. Chinchanikar S, Choudhury SK (2013) Investigations on machinability aspects of hardened AISI 4340 steel at different levels of hardness using coated carbide tools. Int J Refract Met Hard Mater 38:124–133

24. Gong F, Zhao J, Pang JM (2017) Evolution of cutting forces and tool failure mechanisms in intermittent turning of hardened steel with ceramic tool. Int J Adv Manuf Technol 89(5–8):1603–1613

25. Niu QL, Chen M, Ming WW, An QL (2013) Evaluation of the performance of coated carbide tools in face milling TC6 alloy under dry condition. Int J Adv Manuf Technol 64(5–8):623–631